Current Biology 23, 828–834, May 6, 2013 ©2013 Elsevier Ltd All rights reserved http://dx.doi.org/10.1016/j.cub.2013.03.068

Report

Myosin-V Opposes Microtubule-Based Cargo Transport and Drives Directional Motility on Cortical Actin

Lukas C. Kapitein,[1,2,*] Petra van Bergeijk,[1] Joanna Lipka,[1,3] Nanda Keijzer,[2] Phebe S. Wulf,[1,2] Eugene A. Katrukha,[1] Anna Akhmanova,[1] and Casper C. Hoogenraad[1,2,*]
[1]Division of Cell Biology, Department of Biology, Faculty of Science, Utrecht University, 3584 CH Utrecht, the Netherlands
[2]Department of Neuroscience, Erasmus Medical Center, 3015 GE Rotterdam, The Netherlands
[3]International Institute of Molecular and Cell Biology, 02-109 Warsaw, Poland

Summary

Intracellular transport is driven by motor proteins that either use microtubules or actin filaments as their tracks [1], but the interplay between these transport pathways is poorly understood [2–4]. Whereas many microtubule-based motors are known to drive long-range transport, several actin-based motors have been proposed to function predominantly in cargo tethering [4–6]. How these opposing activities are integrated on cargoes that contain both types of motors is unknown. Here we use inducible intracellular transport assays to show that acute recruitment of myosin-V to kinesin-propelled cargo reduces their motility near the cell periphery and enhances their localization at the actin-rich cell cortex. Myosin-V arrests rapid microtubule-based transport without the need for regulated auto- or other inhibition of kinesin motors. In addition, myosin-V, despite being an ineffective long-range transporter, can drive slow, medium-range (1–5 μm), point-to-point transport in cortical cell regions. Altogether, these data support a model in which myosin-V establishes local cortical delivery of kinesin-bound cargos through a combination of tethering and active transport.

Results and Discussion

The unconventional myosin motor myosin-V has clear transporting roles in yeast and plants [7–11], but direct evidence for myosin-V-driven point-to-point transport in vertebrate cells is surprisingly limited [2, 4]. In these cells, microtubule-based motor proteins mediate most long-range transport, and myosin-V-dependent vectorial transport has only been directly demonstrated in specialized structures with distinct actin organization, such as dendritic spines [12–14]. In contrast, experiments in which the intracellular motility of quantum dot-labeled myosin-V was examined showed very short directional runs (<1 s), whereas motility at longer timescales was random [15]. Myosin-V-dependent melanosome movements have also been reported, but the extent to which these movements were dependent on myosin-V stepping, rather than dynamics of the actin cytoskeleton, has remained unclear [4, 6, 16]. Thus, it remains uncertain whether myosin-V motors can drive directional cargo transport over longer distances on the nonuniform, disorganized actin cytoskeleton of mammalian cells [2, 4]. Several models instead propose a role for myosin-V in tethering of cargo transported by microtubule-based motors [2, 4, 5, 17, 18], but whether the presence of myosin-V is sufficient to stall microtubule-based cargo motility is not known.

To directly probe the intracellular activity of myosin-V in fibroblast cells, we created a fusion construct of GFP and myosin-V, which was truncated such that it contained the motor domain and dimerization (coiled-coil) region but lacked the known cargo-binding domain [2, 19, 20] (MyoVb[1–1090]-GFP-FRB, hereafter called "myosin-V"; Figure 1A). Upon expression in COS7 cells, myosin-V was highly enriched in actin-rich protrusions at the cell border (see Figure S1A available online). This specific distribution could be a consequence of motor activity toward the actin barbed end or represent a specific affinity for the actin present in these protrusions. To discriminate between these possibilities, we constructed a catalytically impaired motor (MyoVb[1–1090;G441A]-GFP-FRB [21], hereafter called "rmyosin-V," from "rigor"; Figure 1A) and found no enrichment at the cell border (Figure S1B). In addition, because processive motor activity requires two coordinated motor domains, we also created MyoVb(1–893)-GFP-FRB, a construct lacking the dimerization domain. Again, no accumulation at the cell border was observed upon expression of this monomeric myosin construct (mmyosin-V, Figure S1C). In contrast, strong cortical accumulation of the shorter construct could be stimulated by chemically induced mmyosin-V dimer formation using the FKBP-rapalog-FRB system (Figures S1D and S1E), indicating that dimeric myosin-V can move processively inside live COS7 cells.

To further examine the intracellular dynamics of non-cargo-bound myosin-V, we performed time-lapse microscopy in cells expressing myosin-V together with CDC42 to enhance formation of filopodia rich in uniformly barbed-end, out-oriented actin [22, 23] (Figure S1F). Remarkably, although clear myosin-V accumulation at the tips could be observed, the most apparent motility was directed inward and was similar to the retrograde flow observed for actin (Figure S1G). We next photobleached intermediate segments of filopodia to test for directional motility into filopodia and observed two modes of motility into the photobleached area, as expected from numerical simulations (Figure S1H). Myosin-V entered the distal part of the bleached area at the expected velocity of ~30 nm/s, whereas motility from the cell body into the filopodia occurred at the faster rate of ~300 nm/s (Figure S1I). Interestingly, many of the newly entered myosin-V motors changed behavior in the bleached zone and started drifting back to the cell body at the slow rate (Figure S1I). Similar behaviors were observed for chemically dimerized mmyosin-V (Figures S1J and S1K). Together, these data demonstrate that individual myosin-V dimers alternate between active and passive actin-binding modes.

To directly probe the activity of myosin-V bound to cargo, we employed our recently developed intracellular cargo-trafficking assay [24]. In this assay, we employ the FKBP-rapalog-FRB heterodimerization system to induce specific motor protein recruitment to peroxisomes during live-cell recordings (Figure 1B). Because peroxisomes are largely immobile in the perinuclear region before rapalog addition (Movies S2 and S3), their motility after rapalog addition selectively reports

*Correspondence: l.kapitein@uu.nl (L.C.K.), c.hoogenraad@uu.nl (C.C.H.)

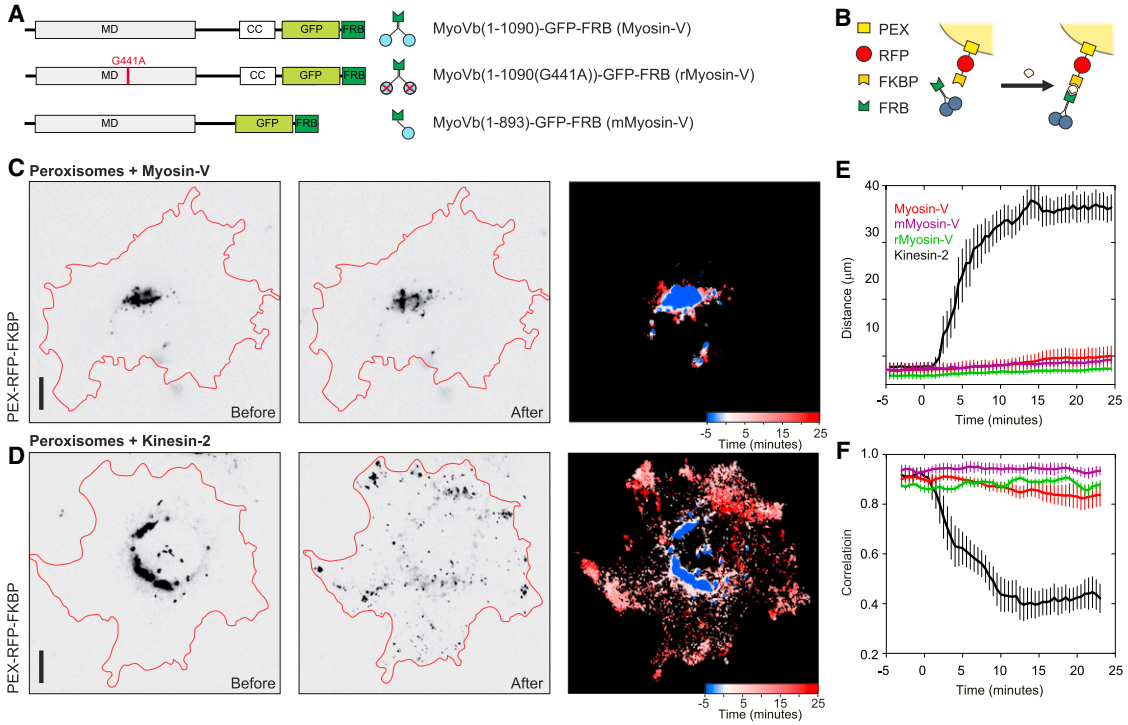

Figure 1. Intracellular Dynamics of Dimeric, Monomeric, and Catalytically Impaired Myosin-V Constructs

(A) Overview of myosin-V constructs used in this study.

(B) Assay: a fusion construct of PEX3, RFP, and FKBP targets peroxisomes. Fusion of FRB with truncated motor construct (myosin-V or kinesin-2) is recruited to FKBP and consequently the peroxisomes upon addition of rapalog.

(C and D) Peroxisome distribution before and after recruitment of myosin-V (C) or kinesin-2 (D) by rapalog addition (inverted contrast). Yellow curves indicate cell outline. Each third panel depicts an overlay of sequential binarized images from the respective recordings, color coded by time as indicated. Blue marks the initial distribution, whereas red marks regions targeted upon addition of rapalog. See Movie S2.

(E and F) Average time traces of the $R_{90\%}$ (radius of circle enclosing 90% of cellular fluorescence; see Experimental Procedures) (E) and the frame-to-frame correlation index (F) for peroxisomes in COS7 cells expressing myosin-V (red, see C, n = 6 cells), mmyosin-V (cyan, n = 4 cells), rmyosin-V (green, n = 7 cells), or kinesin-2 (black, see D, n = 10), to which rapalog is added at time point 0.

Error bars depict SE. Scale bars represent 10 μm.

the activity of the specific FRB-tagged motor that was recruited. Whereas peroxisomes rapidly redistributed to the cell periphery upon recruitment of the plus-end-directed, microtubule-based motor kinesin-1 (KIF5, data not shown [24, 25]) or kinesin-2 (KIF17, Figure 1D), very little peroxisome motility was observed upon chemically induced recruitment of myosin-V (Figure 1C). To quantify these effects, we calculated for each time point the radius required to include 90% of all fluorescence intensity from the peroxisomes, $R_{90\%}$ [24], and found a large increase upon recruitment of kinesin-2, whereas $R_{90\%}$ hardly changed upon recruitment of myosin-V, rmyosin-V, or mmyosin-V (Figure 1E). These data indicate that myosin-V, when recruited to cargo in the perinuclear region, is not an effective long-range transporter inside live COS7 cells.

The lack of robust cargo motility driven by myosin-V could reflect an alternative role for myosin-V on cargo, such as opposing microtubule-based motor proteins. Importantly, we observed that most kinesin-propelled peroxisomes never stopped moving after reaching the cell periphery but instead continued to be mobile (Figure 1D). To quantify this observation, we used image correlation analysis [26] to measure the overall frame-to-frame differences in our recordings. The average correlation index $c_{30}(t)$ was calculated for each 30 s interval within a moving window of six frames to determine how the peroxisome motility changed over time. A correlation of 1 indicates that two images are completely identical, whereas 0 indicates that the intensity is distributed over a completely different set of pixels. Recruitment of kinesin-2 to peroxisomes caused a persistent drop in correlation c_{30} from 0.91 ± 0.02 to 0.42 ± 0.06 (mean ± SD, n = 10 cells), reflecting the rapid displacement of peroxisomes (Figure 1F). Consistent with our primary observations, the correlation index remained low even after arrival in the cell periphery. Only upon depolymerization of microtubules using nocodazole did the correlation index rapidly increase, reflecting that kinesin-driven motility was now prohibited (Figures S2A and S2B). These results demonstrate that kinesin-2 continues to drive rapid motility of cargo near the cell periphery.

To test how myosin-V affects the motility of cargo driven by microtubule-based motor proteins, we next recruited kinesin-2 to peroxisomes together with myosin-V or rmyosin-V (Figure 2A). Peroxisomes again rapidly moved outward in most cells (Figures 2B and 2E), but now most peroxisomes stopped at the cell border, where they became strongly colocalized with myosin-V (Figures 2B–2D). Calculation of the correlation index over time revealed that, for both myosin-V and rmyosin-V, the initial rapid drop upon addition of rapalog was now followed by an increase when peroxisomes reached the cell periphery, reflecting the reduced motility (Figures 2F and

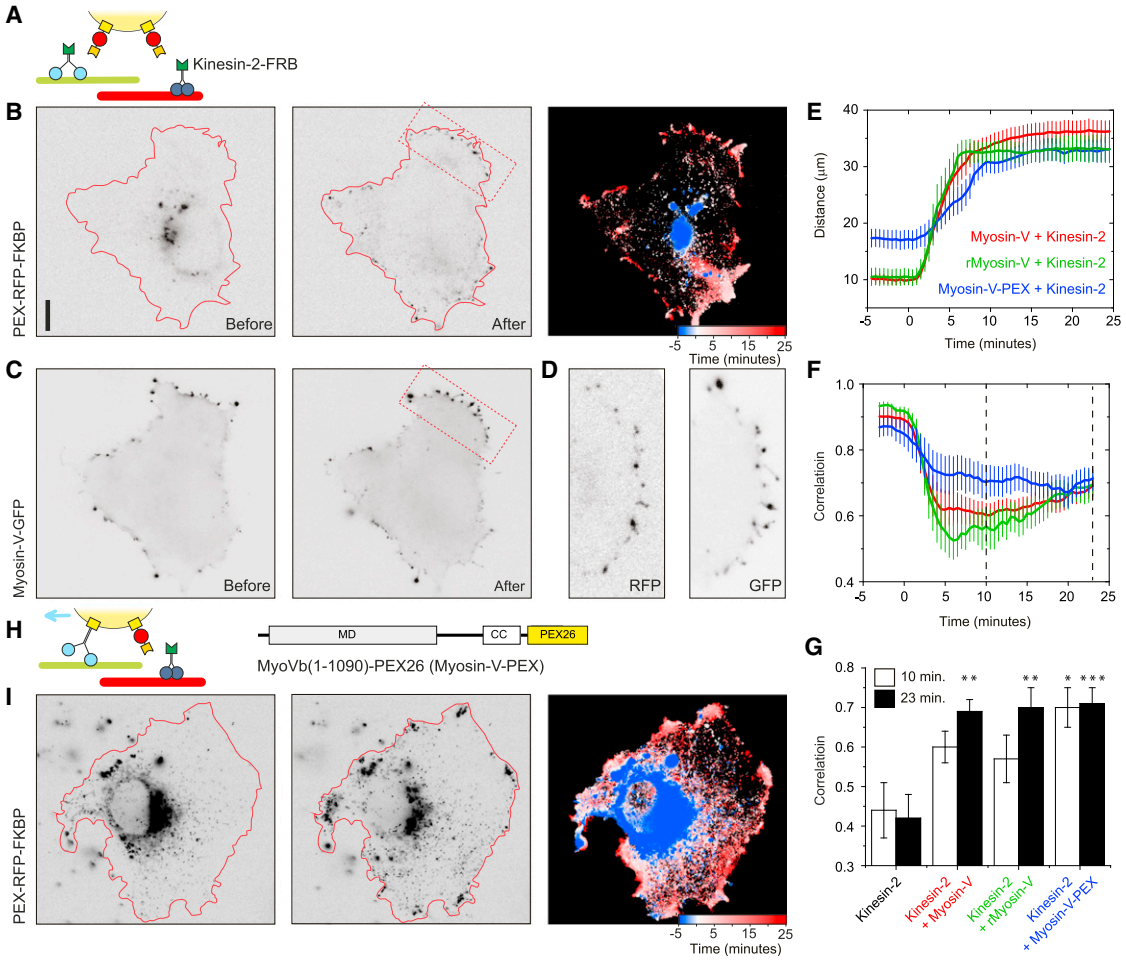

Figure 2. Myosin-V Anchors Kinesin-Propelled Cargo near the Cell Periphery

(A) Assay: two different motors are recruited to the peroxisomes upon addition of rapalog.

(B) Peroxisome distribution before and after recruitment of myosin-V and kinesin-2 by rapalog addition. Yellow curves indicate cell outline. Third panel depicts an overlay of sequential binarized images from the respective recordings, color coded by time as indicated. See Movie S3.

(C) Distribution of MyoVb(1–1090)-GFP-FRB before and after addition of rapalog.

(D) Enlargement of the regions marked in red in (B) and (C).

(E and F) Average time traces of the $R_{90\%}$ (E) and the frame-to-frame correlation index (F) versus time for peroxisomes in COS7 cells expressing kinesin-2 together with myosin-V (red, n = 17 cells), rmyosin-V (green, n = 7 cells) or MyoVb(1–1090)-PEX26 (blue, n = 16 cells). Dotted line marks time points used for (G).

(G) Average correlation at 10 and 23 min after rapalog addition for the indicated experiments. Asterisks depict p values obtained from t tests of values against control with KIF17 only (*$p < 0.01$; **$p < 0.005$; ***$p < 0.001$).

(H) Assay: kinesin-2 is recruited to peroxisomes preloaded with myosin-V using the fusion construct MyoVb(1–1090)-PEX26 (PEX26 to allow a fusion at the C terminus of myosin-V).

(I) Peroxisome distribution before and after rapalog addition to recruit kinesin-2 to myosin-V-coated peroxisomes. Yellow curves indicate cell outline. Third panel depicts an overlay of sequential binarized images from the respective recordings, color coded by time as indicated.

Contrast is inverted for all fluorescence images. Error bars depict SE. Scale bars represent 10 μm.

2G). This selective peripheral anchoring by myosin-V could reflect that myosin-V recruitment to peroxisomes is inefficient in regions where it is not enriched. To test whether myosin-V could oppose kinesin-based motility throughout the whole cell if recruited at sufficiently high levels, we recruited kinesin-2 to peroxisomes that were preloaded with myosin-V through a direct fusion with the peroxisomal protein PEX26 (Figures 2H and 2I). Kinesin-2-driven displacement to the cell periphery was now decelerated (Figure 2E), and the correlation index was high throughout the cell and not only when peroxisomes reached the cell periphery (Figures 2F and 2G). These results demonstrate that myosin-V can oppose kinesin-driven motility throughout the cell.

To specifically probe how acute myosin-V recruitment affects the motility of kinesin-propelled cargo, we next used a fusion construct of kinesin-2 and PEX26 that, upon expression, induced the radial redistribution of peroxisomes (Figures 3A and 3B). Similar to the experiment where kinesin-2 was recruited by rapalog addition, these peroxisomes were not immobile near the cell periphery but kept changing positions, as reflected in the low correlation index of 0.43 ± 0.05 (Figure 3F). When myosin was recruited to these motile peroxisomes, their dynamics slowed down dramatically (Figures 3B–3F). The observed increase in the correlation index from 0.42 ± 0.07 (at 0:00) to 0.65 ± 0.07 (at 23 min after rapalog addition) was only slightly less than the effect of complete microtubule

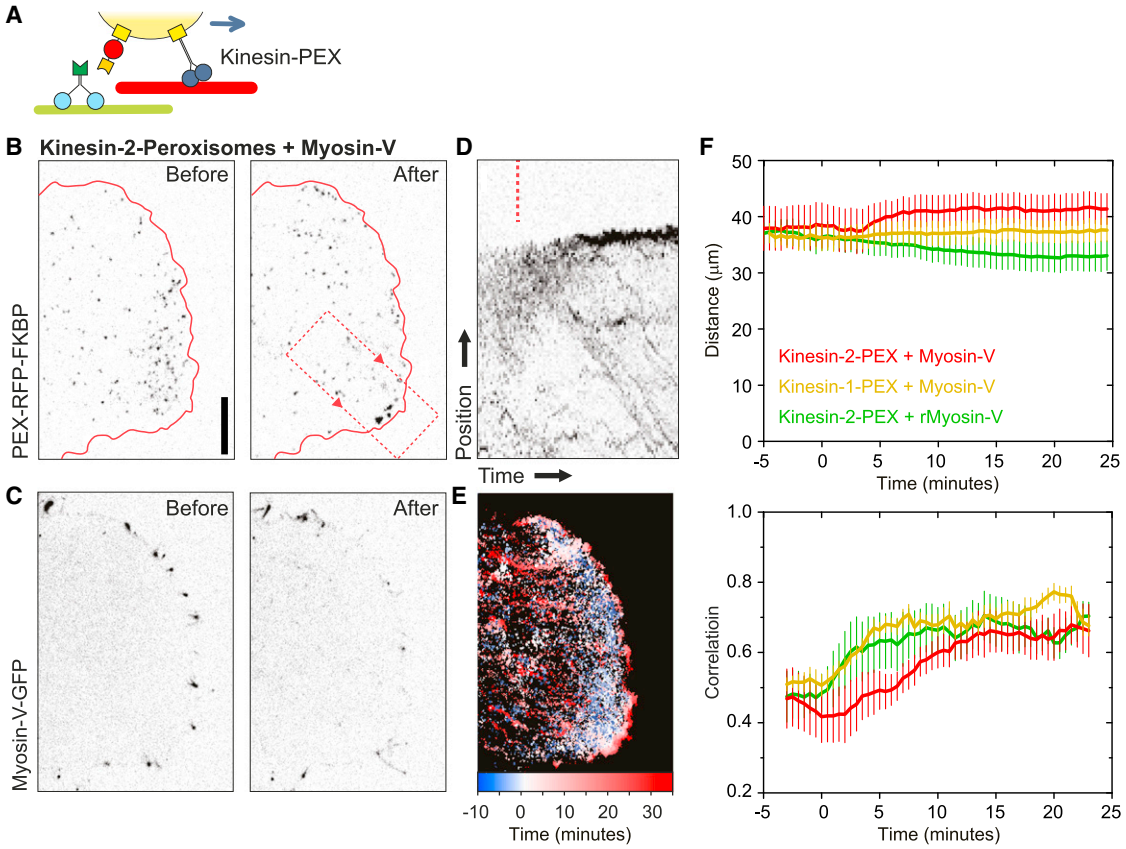

Figure 3. Acute Recruitment of Myosin-V to Kinesin-Propelled Cargo at the Cell Periphery

(A) Assay: a fusion construct PEX26 with either kinesin-1 or kinesin-2 targets peroxisomes and redistributes them throughout the cell. PEX-RFP-FKBP also targets these peroxisomes and recruits myosin-V upon addition of rapalog.

(B and C) Peroxisome (B) and myosin-V (C) distributions before and after recruitment of myosin-V to kinesin-2-propelled peroxisomes by rapalog addition. Box indicates region used for kymography in (D). See also Movie S4.

(D) Kymograph of the recordings shown in (B). Dotted line marks rapalog addition.

(E) Overlay of sequential binarized images from the recording in (B), color coded by time as indicated.

(F) Time traces of the $R_{90\%}$ (distance, top) and the frame-to-frame correlation index (bottom) versus time for peroxisomes in COS7 cells expressing kinesin-2-PEX together with myosin-V (red, n = 6 cells) or rmyosin-V (green, n = 4 cells), or kinesin-1-PEX together with myosin-V (yellow, n = 5 cells). Rapalog is added at time point 0. For this analysis, only peroxisomes located in the outer 10–20 μm of the cell were included.

Contrast is inverted for all fluorescence images. Error bars depict SE. Scale bars represent 10 μm.

depolymerization (from 0.5 ± 0.15 to 0.8 ± 0.04; see Figure S2B). However, in addition to the attenuation of microtubule-based motility, two effects could be distinguished. A subset of peroxisomes now appeared at the cell edge, where they colocalized with myosin-V, whereas the other peroxisomes slowly moved away from the cell edge (Figures 3B–3E). Similar results were obtained when myosin-V was recruited to peroxisomes propelled by the kinesin-1 family member KIF5B (Figure 3F). In contrast, although recruitment of rmyosin-V was sufficient to arrest kinesin-driven motility, it did not result in cargo accumulation at the cell edge, suggesting that peripheral accumulation requires active motility of myosin-V (Figure 3F).

To directly test for directional myosin-V-driven transport at the cell periphery of vertebrate cells, we repeated the dual-motor assay but now incubated cells with the microtubule-depolymerizing agent nocodazole before the start of the experiment to stop kinesin-2-driven peroxisomal motility (Figures 4A, S2A, and S2B). Recruitment of dimeric myosin-V, but not rmyosin-V, resulted in the persistent directional motility of many peroxisomes toward the cell edge (Figures 4B–4N). Furthermore, recruitment of (multiple) monomeric myosin-V motors was also sufficient to induce directional motility of peroxisomes to the cell edge (Figures S2C–S2H). Finally, to maintain cytoskeletal integrity and stop kinesin-driven motility without microtubule depolymerization, we used specific chemical inhibition of kinesin-5-PEX26 using S-trityl-L-cysteine (STLC) [27, 28] before addition of rapalog and again observed directional motility driven upon recruitment of myosin-V (Figures S2J–S2P). These results directly demonstrate that, in contrast to the metabolically impaired rmyosin-V, myosin-V can drive medium-range point-to-point transport (>1 μm) toward the cell edge in mammalian cells.

To quantify these results, we traced individual peroxisomes linked to either myosin-V or rmyosin-V, averaged their mean-squared displacements (MSD) for different time intervals τ, and found that myosin-V induced more motility than rmyosin-V (Figures 4N and 4O). The power dependence α of the MSD with increasing time intervals τ, MSD $\propto \tau^{\alpha}$, is the anomalous diffusion exponent [15, 29] and indicates whether motility is completely random ($\alpha \approx 1$, diffusive), directed ($1 < \alpha \leq 2$, superdiffusive), or confined ($0 < \alpha < 1$, subdiffusive). The overall myosin-V-driven peroxisome motility

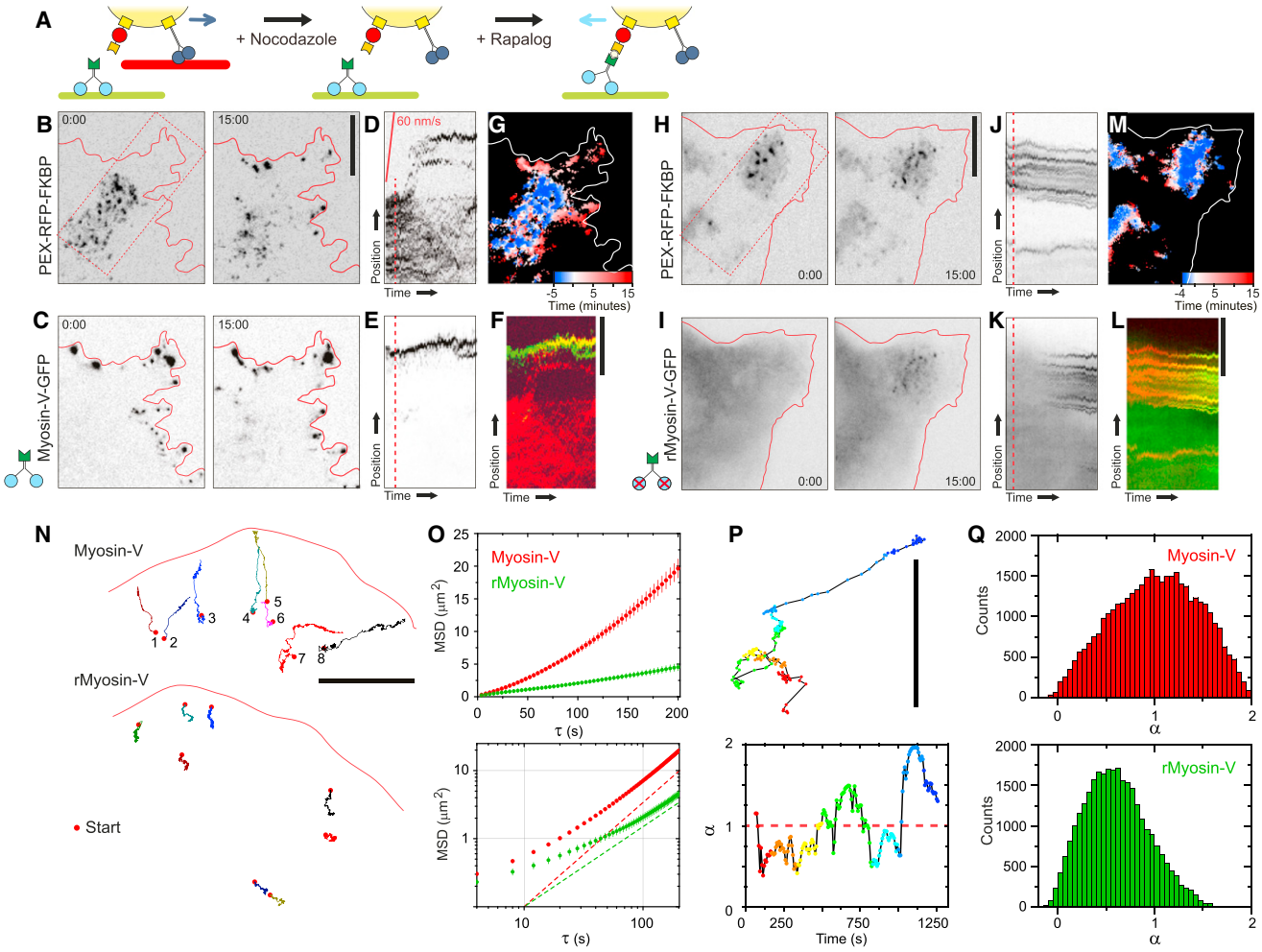

Figure 4. Myosin-V Can Autonomously Drive Directional Cargo Motility near the Cell Periphery

(A) Assay: peroxisomes are preloaded with kinesin-2 to induce peripheral distribution. After microtubule depolymerization by nocodazole addition, rapalog is added to recruit myosin-V.

(B and C) Frames from a time-lapse recording of peroxisomes (B) and myosin-V (C) for the assay depicted in (A). Time point 0:00 marks the addition of rapalog. Box indicates region used for kymography in (D) and (E). See Movie S5.

(D and E) Kymograph of the recordings shown in (B) and (C), respectively. Dotted line marks rapalog addition.

(F) Pseudocolored merge of (D) and (E).

(G) Overlay of sequential binarized images from the recording in (B), color coded by time as indicated.

(H and I) Frames from a time-lapse recording of peroxisomes (H) and rmyosin-V (I) for the assay depicted in (A). Time point 0:00 marks the addition of rapalog. Box indicates region used for kymography in (J) and (K).

(J and K) Kymograph of the recordings shown in (H) and (I), respectively. Dotted line marks rapalog addition.

(L) Pseudocolored merge of (J) and (K).

(M) Overlay of sequential binarized images from the recording in (B), color coded by time as indicated.

(N) Example trajectories of peroxisomes linked to myosin-V (top) or rmyosin-V (bottom) near the cell edge (marked in red). Red dot marks start of the trajectory. Data was acquired with 4 s intervals. Total time of trajectory: 1, 7:04; 2, 7:48; 3, 24:36; 4, 17:16; 5, 6:00; 6, 9:40; 7, 30:00; 8, 30:00. 16:44 for all trajectories of rmyosin-V. See Movie S6.

(O) Average mean-squared displacement calculated from trajectories of peripherally located peroxisomes linked to either myosin-V or rmyosin-V, plotted with linear (top) or logarithmic axes (bottom). n = 285 and 168 trajectories for myosin-V and rmyosin-V, respectively.

(P) Example trajectory, color coded for time from red to blue as indicated in the windowed $\alpha_{0-28\ s}(t)$ trace shown at bottom.

(Q) Histograms of α_{0-28} s obtained from 38,426 and 29,937 28 s intervals from 285 and 168 different trajectories of myosin-V and rmyosin-V, respectively. Contrast is inverted for all fluorescence images. Scale bars represent 10 μm, except in (N) and (P), where scale bars represent 5 μm.

was superdiffusive (slope in log-log plot > 1, Figure 4O), whereas motility in the presence of rmyosin-V was subdiffusive at short time scales ($\tau < 100$ s) and superdiffusive at longer time scales as a result of slow movement away from the cell edge (Figure 4N). However, directed motility of myosin-V was also often interspersed with long pauses or more random movements (Figures 4N and 4P). We therefore further analyzed peroxisome trajectories by calculating the MSD(τ) and α for a sliding window of 28 s to examine how α(t) varied over time (Figures 4P and 4Q). This analysis revealed that peroxisome motility was often subdiffusive for many minutes ($<\alpha> = 1.0 \pm 0.5$, mean ± SD, Figures 4P and 4Q). Nevertheless, many intervals were classified as superdiffusive episodes ($\alpha > 1$), whereas for rmyosin-V most intervals were subdiffusive

($<\alpha> = 0.6 \pm 0.4$, mean ± SD, Figure 4Q). Thus, myosin-V can drive directional transport.

In this study, we have provided direct evidence for myosin-V-driven directional cargo transport at the cell periphery, demonstrating that the dynamic and irregular peripheral actin organization still supports robust actin-based directional motility. Despite the overall directionality toward the cell edge, myosin-V-mediated motility was highly irregular and frequently halted for long periods, consistent with earlier work showing that most myosin-V-based motility is effectively random at 1–5 s time scales [15]. In addition, we have shown that acute recruitment of myosin-V to kinesin-propelled cargo is sufficient to attenuate their motility. These results are consistent with the pioneering study of melanosome dynamics in mouse melanocytes, where myosin-Va was shown to dampen both speed and length of microtubule-based runs [6]. Similar results have also been reported for mitochondria and secretory granules in neurons [17, 30] and recycling endosomes in HeLa cells [5]. The immediate stalling of kinesin-driven cargo observed upon stochastic coupling of myosin-V demonstrates a kinesin inactivation scheme alternative to regulated unbinding or auto- or other inhibition.

Our model system provides a well-controlled method to examine the interplay between different types of motors inside cells but (intentionally) does not incorporate all aspects known to regulate motor activity. For example, the use of constitutively active and permanently attached myosin-V and kinesin bypasses the regulatory layer in which specific adaptor molecules, such as melanophilin, and specific posttranslational modifications, such as phosphorylation, regulate motor attachment and conformation [2, 31, 32]. Future work will be needed to better understand how myosin-V activity is controlled [13] and how the outcome of motor antagonism depends on the precise numbers of motors involved [33]. The approach introduced here will be an important starting point for such developments.

Experimental Procedures

DNA Constructs

The DNA constructs used in this study are cloned in pGW1-CMV or pβactin-16-pl. Myosin-V-(1–1090)-GFP-FRB (myosin-V), myosin-V-(1–1090;G441A)-GFP-FRB (rmyosin-V), and myosin-V-(1–893)-GFP-FRB (mmyosin-V) were made by PCR from mouse myosin-Vb cDNA (NM_201600), purchased from Geneservice (IMAGE 40099275). PEX3 and PEX26 constructs were described previously [24]. For details, see Supplemental Experimental Procedures.

Cell Cultures, Live-Cell Image Acquisition, and Image Processing and Analysis

COS7 were cultured in DMEM/Ham's F10 (50%/50%) medium containing 10% FCS and 1% penicillin/streptomycin. Cells were plated on 24 mm diameter coverslips and 2–3 days later transfected with FuGENE6 transfection reagent (Roche). Time-lapse live-cell imaging was performed on an Eclipse TE2000E (Nikon) equipped with a CoolSNAP HQ (Photometrics) camera and an incubation chamber (Tokai Hit; INUG2-ZILCS-H2) mounted on a motorized stage (Prior). COS7 cells were imaged in Ringer's solution at 37°C. During image acquisition, rapalog was added to establish a final rapalog concentration of 100 nM. Images of live cells were processed and analyzed using MetaMorph (Molecular Devices) and LabVIEW (National Instruments) software. For details, see Supplemental Experimental Procedures.

Supplemental Information

Supplemental Information includes two figures, Supplemental Experimental Procedures, and six movies and can be found with this article online at http://dx.doi.org/10.1016/j.cub.2013.03.068.

Acknowledgments

We are grateful to N. Hussain for Cdc42-myc cDNA, to Y. Hayashi for GFP-actin cDNA, and to Ariad Pharmaceuticals for FKBP/FRB cDNAs and rapalog (AP21967). J.L. is supported by the International Ph.D. Projects Program of Foundation for Polish Science (Studies of Nucleic Acids and Proteins—from Basic to Applied Research), cofinanced by the European Union, Regional Development Fund, and cosupervised by J. Jaworski. This work was supported by the Erasmus Medical Center (EMC fellowship to L.C.K.) and the Netherlands Organisation for Scientific Research (NWO-ALW-VENI to L.C.K., NWO-ALW-VICI to A.A. and C.C.H., and NWO-nano to L.C.K. and C.C.H.), the Netherlands Organisation for Health Research and Development (ZonMW-TOP to A.A. and C.C.H.), and EMBO Young Investigators Program (YIP to C.C.H.). This research is also supported by the Dutch Technology Foundation STW, which is part of the Netherlands Organisation for Scientific Research (NWO), and which is partly funded by the Ministry of Economic Affairs.

Received: September 27, 2012
Revised: February 27, 2013
Accepted: March 28, 2013
Published: April 18, 2013

References

1. Vale, R.D. (2003). The molecular motor toolbox for intracellular transport. Cell *112*, 467–480.
2. Hammer, J.A., 3rd, and Sellers, J.R. (2011). Walking to work: roles for class V myosins as cargo transporters. Nat. Rev. Mol. Cell Biol. *13*, 13–26.
3. Ross, J.L., Ali, M.Y., and Warshaw, D.M. (2008). Cargo transport: molecular motors navigate a complex cytoskeleton. Curr. Opin. Cell Biol. *20*, 41–47.
4. Woolner, S., and Bement, W.M. (2009). Unconventional myosins acting unconventionally. Trends Cell Biol. *19*, 245–252.
5. Provance, D.W., Jr., Addison, E.J., Wood, P.R., Chen, D.Z., Silan, C.M., and Mercer, J.A. (2008). Myosin-Vb functions as a dynamic tether for peripheral endocytic compartments during transferrin trafficking. BMC Cell Biol. *9*, 44.
6. Wu, X., Bowers, B., Rao, K., Wei, Q., and Hammer, J.A., 3rd. (1998). Visualization of melanosome dynamics within wild-type and dilute melanocytes suggests a paradigm for myosin V function In vivo. J. Cell Biol. *143*, 1899–1918.
7. Schott, D.H., Collins, R.N., and Bretscher, A. (2002). Secretory vesicle transport velocity in living cells depends on the myosin-V lever arm length. J. Cell Biol. *156*, 35–39.
8. Pruyne, D., Legesse-Miller, A., Gao, L., Dong, Y., and Bretscher, A. (2004). Mechanisms of polarized growth and organelle segregation in yeast. Annu. Rev. Cell Dev. Biol. *20*, 559–591.
9. Verchot-Lubicz, J., and Goldstein, R.E. (2010). Cytoplasmic streaming enables the distribution of molecules and vesicles in large plant cells. Protoplasma *240*, 99–107.
10. Peremyslov, V.V., Prokhnevsky, A.I., and Dolja, V.V. (2010). Class XI myosins are required for development, cell expansion, and F-Actin organization in Arabidopsis. Plant Cell *22*, 1883–1897.
11. Zhang, J., Tan, K., Wu, X., Chen, G., Sun, J., Reck-Peterson, S.L., Hammer, J.A., 3rd, and Xiang, X. (2011). Aspergillus myosin-V supports polarized growth in the absence of microtubule-based transport. PLoS ONE *6*, e28575.
12. Wagner, W., Brenowitz, S.D., and Hammer, J.A., 3rd. (2011). Myosin-Va transports the endoplasmic reticulum into the dendritic spines of Purkinje neurons. Nat. Cell Biol. *13*, 40–48.
13. Wang, Z., Edwards, J.G., Riley, N., Provance, D.W., Jr., Karcher, R., Li, X.D., Davison, I.G., Ikebe, M., Mercer, J.A., Kauer, J.A., and Ehlers, M.D. (2008). Myosin Vb mobilizes recycling endosomes and AMPA receptors for postsynaptic plasticity. Cell *135*, 535–548.
14. Schuh, M. (2011). An actin-dependent mechanism for long-range vesicle transport. Nat. Cell Biol. *13*, 1431–1436.
15. Nelson, S.R., Ali, M.Y., Trybus, K.M., and Warshaw, D.M. (2009). Random walk of processive, quantum dot-labeled myosin Va molecules within the actin cortex of COS-7 cells. Biophys. J. *97*, 509–518.
16. Gross, S.P., Tuma, M.C., Deacon, S.W., Serpinskaya, A.S., Reilein, A.R., and Gelfand, V.I. (2002). Interactions and regulation of molecular motors in Xenopus melanophores. J. Cell Biol. *156*, 855–865.

17. Pathak, D., Sepp, K.J., and Hollenbeck, P.J. (2010). Evidence that myosin activity opposes microtubule-based axonal transport of mitochondria. J. Neurosci. *30*, 8984–8992.
18. Desnos, C., Huet, S., and Darchen, F. (2007). 'Should I stay or should I go?': myosin V function in organelle trafficking. Biol. Cell *99*, 411–423.
19. Liu, J., Taylor, D.W., Krementsova, E.B., Trybus, K.M., and Taylor, K.A. (2006). Three-dimensional structure of the myosin V inhibited state by cryoelectron tomography. Nature *442*, 208–211.
20. Thirumurugan, K., Sakamoto, T., Hammer, J.A., 3rd, Sellers, J.R., and Knight, P.J. (2006). The cargo-binding domain regulates structure and activity of myosin 5. Nature *442*, 212–215.
21. Yengo, C.M., De la Cruz, E.M., Safer, D., Ostap, E.M., and Sweeney, H.L. (2002). Kinetic characterization of the weak binding states of myosin V. Biochemistry *41*, 8508–8517.
22. Hussain, N.K., Jenna, S., Glogauer, M., Quinn, C.C., Wasiak, S., Guipponi, M., Antonarakis, S.E., Kay, B.K., Stossel, T.P., Lamarche-Vane, N., and McPherson, P.S. (2001). Endocytic protein intersectin-l regulates actin assembly via Cdc42 and N-WASP. Nat. Cell Biol. *3*, 927–932.
23. Nobes, C.D., and Hall, A. (1995). Rho, rac, and cdc42 GTPases regulate the assembly of multimolecular focal complexes associated with actin stress fibers, lamellipodia, and filopodia. Cell *81*, 53–62.
24. Kapitein, L.C., Schlager, M.A., van der Zwan, W.A., Wulf, P.S., Keijzer, N., and Hoogenraad, C.C. (2010). Probing intracellular motor protein activity using an inducible cargo trafficking assay. Biophys. J. *99*, 2143–2152.
25. Kapitein, L.C., Schlager, M.A., Kuijpers, M., Wulf, P.S., van Spronsen, M., MacKintosh, F.C., and Hoogenraad, C.C. (2010). Mixed microtubules steer dynein-driven cargo transport into dendrites. Curr. Biol. *20*, 290–299.
26. Kolin, D.L., and Wiseman, P.W. (2007). Advances in image correlation spectroscopy: measuring number densities, aggregation states, and dynamics of fluorescently labeled macromolecules in cells. Cell Biochem. Biophys. *49*, 141–164.
27. Skoufias, D.A., DeBonis, S., Saoudi, Y., Lebeau, L., Crevel, I., Cross, R., Wade, R.H., Hackney, D., and Kozielski, F. (2006). S-trityl-L-cysteine is a reversible, tight binding inhibitor of the human kinesin Eg5 that specifically blocks mitotic progression. J. Biol. Chem. *281*, 17559–17569.
28. Ally, S., Larson, A.G., Barlan, K., Rice, S.E., and Gelfand, V.I. (2009). Opposite-polarity motors activate one another to trigger cargo transport in live cells. J. Cell Biol. *187*, 1071–1082.
29. Saxton, M.J., and Jacobson, K. (1997). Single-particle tracking: applications to membrane dynamics. Annu. Rev. Biophys. Biomol. Struct. *26*, 373–399.
30. Desnos, C., Huet, S., Fanget, I., Chapuis, C., Böttiger, C., Racine, V., Sibarita, J.B., Henry, J.P., and Darchen, F. (2007). Myosin va mediates docking of secretory granules at the plasma membrane. J. Neurosci. *27*, 10636–10645.
31. Akhmanova, A., and Hammer, J.A., 3rd. (2010). Linking molecular motors to membrane cargo. Curr. Opin. Cell Biol. *22*, 479–487.
32. Karcher, R.L., Deacon, S.W., and Gelfand, V.I. (2002). Motor-cargo interactions: the key to transport specificity. Trends Cell Biol. *12*, 21–27.
33. Derr, N.D., Goodman, B.S., Jungmann, R., Leschziner, A.E., Shih, W.M., and Reck-Peterson, S.L. (2012). Tug-of-war in motor protein ensembles revealed with a programmable DNA origami scaffold. Science *338*, 662–665.